ADVANCED MATERIALS
www.advmat.de

Giant Enhancement of Ferroelectric Retention in $BiFeO_3$ Mixed-Phase Boundary

Yen-Chin Huang, Yunya Liu, Yi-Tsu Lin, Heng-Jui Liu, Qing He, Jiangyu Li, Yi-Chun Chen, and Ying-Hao Chu*

Ferroelectric nano-domains, in which the spontaneous polarization can be controlled by external fields, have attracted considerable interests as media of nonvolatile functional devices. One of the most promising applications is the ferroelectric tunnel junction (FTJ) where the resistance can be modulated along with the polarization orientation, and the resistive readout scheme is non-destructive.[1,2] A large on/off current ratio due to the tunneling electroresistance (TER) effect has been demonstrated in nanoscale FTJs by scanning probe microscopy (SPM);[3–5] moreover, when using ferromagnetic electrodes, spin polarization at the interface can also be affected by the ferroelectric polarization.[6,7] Despite the requirement of an ultrathin tunneling barrier for the TER effect, a recent report has presented the large tunable resistance by either changing the metal conductance of ferroelectric nano-domains[8] or using the tunneling junction between the SPM tip and the ferroelectric surface,[3] which makes relatively thick ferroelectric films applicable for the design. A key issue that has to be solved to realize FTJs is the thermodynamic stability of the domain. Asymmetric free energy landscapes between polarizations directed away and toward the substrates result in at least one unstable polarization state. Such an asymmetry is mainly due to different out-of-plane boundary conditions, such as a nano conducting-tip contact and a bottom electrode. Effects of depolarization fields in the unstable domain become significant when the polarization bound charges are not fully screened.[9] Although efforts on related studies have shown their ways to reduce the energy difference of the polarization double-well by controlling chemical environment,[10] breaking the out-of-plane compositional symmetry,[11–13] or using strain gradient,[14] ferroelectric retention is still a key issue yet to be solved.

In recent studies, researchers have found out that when a $BiFeO_3$ (BFO) film is under a large compressive strain (>4%), the BFO crystal structure transforms into a mixed-phase state of rhombohedrally (R-) and tetragonally (T-) distorted monoclinics. The T/R phase ratio can be manipulated by external voltage, film thickness, or temperature.[15–18] In the mixed-phase BFO film, the stripe-shaped R-BFO is embedded in T-BFO matrix, forming periodic domain pattern with interesting physical properties, such as the large piezo/ferroelectric response[19–21] and the non-zero magnetic moment.[22–24] These mixed-phase boundaries are formed to minimize the elastic and electrostatic energies. In order to shed a light on the retention problem, we intend to use mixed-phase boundaries in BFO as pinning centers for ferroelectric relaxation. Domain wall motions are usually pinned by different kinds of defects, such as charged vacancies,[25–27] dislocations,[28,29] and transient layers with low-magnitude polarization around ferroelastic domains.[30] In this study, the elastic energy term at phase boundaries as topological defects plays an important role to enhance the retention of nano-sized ferroelectric domains. We found out that a stable state of the reversed domain can be achieved when it is pinned by the phase boundaries. The in-plane periodic elastic potentials, instead of out-of-plane electric variables, are used to keep the domain stable. Great improvement on the retention in the mixed-phase system opens a new avenue to ferroelectric retention and the possible application in nanoscale, nonvolatile memory and spintronics. Moreover, the concept of creating long-retention domains by using periodic elastic potential suggests a new way to design strain-mediated FTJs.

The relaxation behaviors of switched domains in the strained BFO film vary with domain-located regions. In topographic images of **Figure 1**a, the flat region is the T-BFO matrix (T-matrix), while the stripe area is the mixed-phase region, where R-BFO is periodically embedded in the T-BFO matrix.[22] The out-of-plane (OP) polarization component of the as-grown film directed downward, i.e. toward the substrate, as shown by the bright contrasts in out-of-plane piezoresponse force microscope (OP-PFM) phase images of Figure 1b. As-grown domains

Y.-C. Huang, Y.-T. Lin, Prof. Y.-C. Chen
Department of Physics
National Cheng Kung University
Tainan 70101, Taiwan
E-mail: ycchen93@mail.ncku.edu.tw
Prof. Y. Y. Liu
School of Materials Science and Engineering
and Key Laboratory of Low Dimensional Materials
& Application Technology of Ministry of Education
Xiangtan University
Xiangtan, Hunan 411105, China
Dr. H.-J. Liu, Prof. Y.-H. Chu
Department of Materials Science and Engineering
National Chiao Tung University
Hsinchu 30010, Taiwan
Prof. Y.-H. Chu
Institute of Physics
Academia Sinica
Taipei 11529, Taiwan
Prof. Q. He
Department of Physics
Durham University
Durham DH1 3LE, UK
Prof. J. Y. Li
Department of Mechanical Engineering
University of Washington
Seattle, WA 98195–2600, USA

DOI: 10.1002/adma.201402442

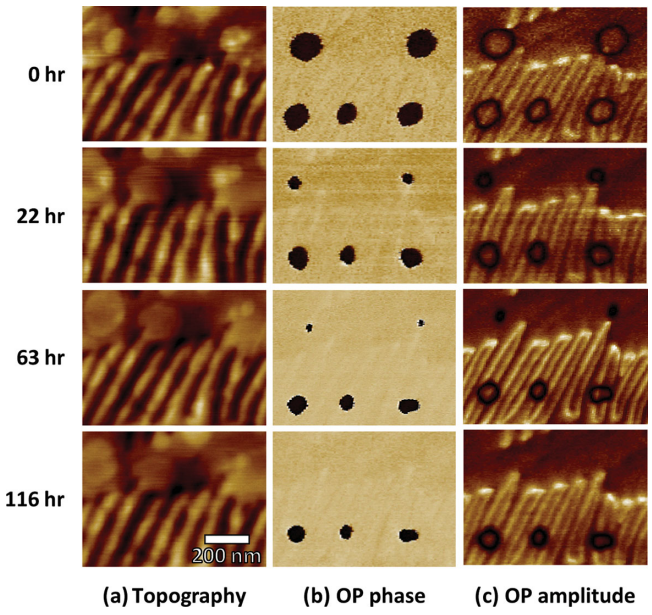

Figure 1. a) Topography, b) OP PFM phase, and c) OP PFM amplitude images of reversed nano domains relaxing toward as-grown states. All domains in T-matrix and mixed phase region were switched by voltage pulses of –15 V tip bias and 100 ms pulse duration. These images were measured just after the domains were switched, and then after 22 hr, 63 hr, and 116 hr.

in mixed phase region form periodically closed loop structures (Figure 1c). The bright closed loops in OP-PFM amplitude images correspond to the T/R-phase boundaries, which separate the R-BFO (inside) and the T-BFO (outside) domains. For domain relaxation study, circular domains were switched point by point in both T-matrix and the mixed-phase region by external voltage pulses with tip bias of –15 V and pulse duration of 100 ms. The dark contrasts of these circular domains in OP-PFM phase images (Figure 1b) indicate that the field-induced domains had reversed OP polarization components directing away from the substrate. The OP-PFM amplitude of the reversed domains is close to that of the as-grown state, and the contrast minimum of the dark circular boundary in Figure 1c was used to determine the position of the domain wall. Figure 1 shows that after 116 hr the reversed domains in T-matrix totally relaxed back to the as-grown state while the reversed domains in the mixed-phase region still kept at finite sizes. It is worth to note that the reversed domain generally decays in a circular shape to reduce the surface energy of the domain wall, but asymmetric strain distribution near the stripe could sometimes deform the shape of the domain from a perfect circle. Tracking PFM images reveals that domains in mixed-phase region relaxed much slower than those in the T-matrix.

Figure 2a shows the comparison of retention behaviors between reversed domains written in the mixed-phase region, T-matrix, and another sample of unstrained BFO film grown on the (001) $SrTiO_3$ substrate. These domains were created by applying external voltage pulses –12 V and pulse duration of 100 ms, and initial domain diameters were about 80~95 nm. Figure 2a indicates that stable reversed domains in mixed-phase region can be maintained much longer than the others, while the relaxation time of domains in strained T-matrix is the shortest. Recent theoretical results have shown that the BFO domain wall energy significantly increases when the film is under a large compressive strain,[31] such as 4% strain from LAO substrate in this study. Therefore, in order to reduce the total free energy, single domain relaxes faster in the strained T-BFO matrix than in the unstrained BFO film. By contrast, in the mixed-phase region, due to the periodic spatial distribution of strain energy, stable reversed domain with very long relaxation time can be obtained by the suitable choice of domain locations. After our testing period of ~307 hr, the reversed domain in mixed-phase region hadn't relaxed to half of its initial size, suggesting that the relaxation time of the stable state was much longer than 307 hr. The mechanism of this long-retention behavior will be discussed in details later. Figure 2b shows a comparison of retention behaviors between reversed domains switched in mixed-phase BFO and other ferroelectrics.[32–41] For the application of nano-sized, nonvolatile data storage, we only considered the reversed domains written by SPM tips in earlier reports and reproduced their relaxation process in the same presentation of normalized retained polarization ratio. These SPM-switched domains all have the same issue of asymmetric out-of-plane boundaries, i.e. different built-in fields between the surface of the film and the interface with the bottom electrodes, so the reversed domains tend to relax to as-grown states. Usually, the domain relaxation time can be extended if the unstable revered domain is written by a longer or higher voltage pulse and formed in a larger initial size. Figure 2b shows that the retention of the reversed domain in mixed-phase region of strained BFO is longer than those of other ferroelectric films even when the domain in mixed-phase BFO is written in a small size (diameter<100 nm) and by a single short pulse (duration time~100 ms).

In order to investigate the mechanism of the superior retention behavior in the mixed-phase region, we have carefully tracked the relaxation processes of a larger domain (diameter>100 nm). **Figure 3** shows a typical curve of the domain diameter versus time for a reversed domain relaxing in the mixed-phase region. The corresponding domain structure to each stage in the relaxation curve is revealed by the PFM image and illustrated by the model diagram, also shown in Figure 3. It is important to note that the size evolution of the domain does not follow a simple exponential decay. For a domain with an initial diameter larger than 100 nm, the domain relaxation speed significantly decreases when the domain decays to a stable size about 80 nm, which is close to the period of as-grown mixed-phase stripes, as shown in the stage from Figure 3c to 3d. OP-PFM image of Figure 3a shows the initial domain structure of a reversed domain induced by a –15 V pulse voltage in the mixed-phase region, where the bright stripes indicated the as-grown T/R-phase boundaries. Higher pulse voltage can reduce depolarization fields inside the domain, and it affects the relaxation rate in the early stage before the domain relaxed to the stable size. In Figure 3a, the left-side wall of the reversed domain was located on a T/R-phase boundary while the right-side domain wall was located within an R-phase domain. Domain relaxation process was not a radially-symmetric decay. From stages (a) to (c) in Figure 3, the reversed domain relaxed fast. During this period, the right-side domain wall moved

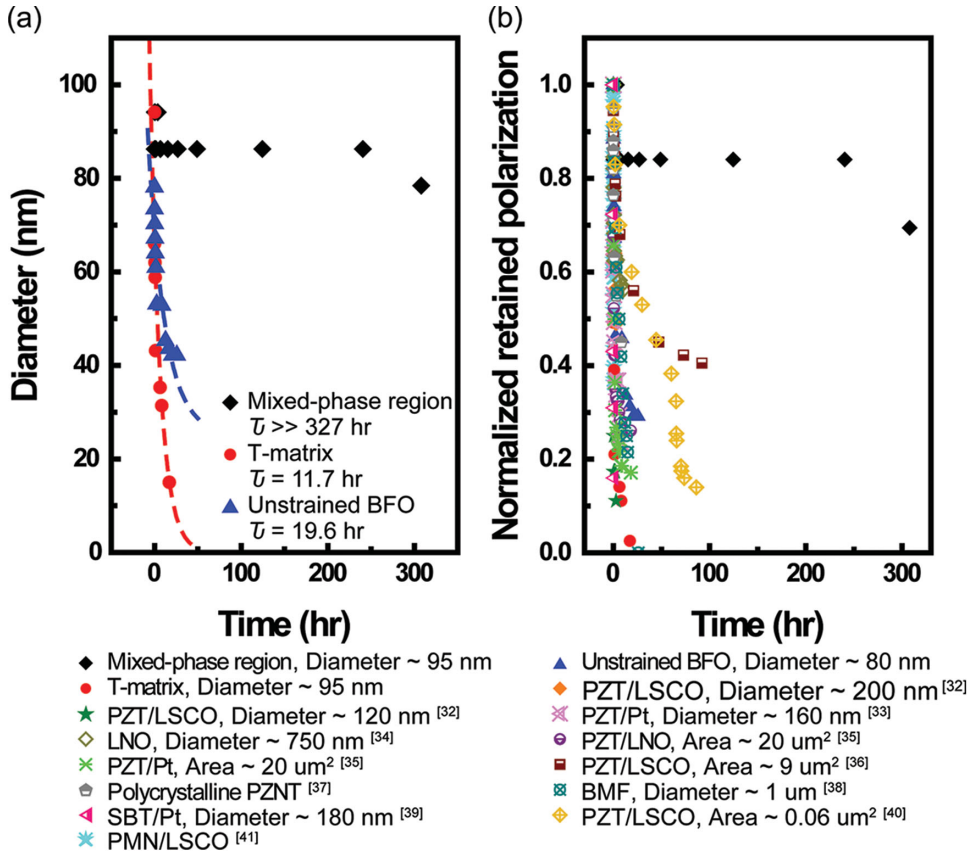

Figure 2. a) Comparison of domain diameters versus the relaxing time between reversed domains switched in the mixed phase region, T-matrix, and unstrained BFO (100) epitaxial film. b) Comparison of normalized retained polarization versus the relaxing time between reversed domains switched in mixed-phase BFO and other ferroelectrics in earlier reports.[32–41]

from inside R-like domain towards a T/R-phase boundary, but the left-side domain wall stayed at the phase boundary. The stable state with both sides of the domain wall located on T/R-phase boundaries can last for a relatively long time (~140 hr) (Figure 3c to 3d). After that, both sides of the domain wall relaxed toward a T/R-phase boundary near the initial center of the reversed domain, and finally, the reversed domain shrank to a dot with a size below the PFM spatial resolution limit. Interestingly, this state of the dot domain could still maintain at least for 24 hr. The stable state in the relaxation process suggests T/R-phase boundaries are pinning centers for the domain wall motion.

In order to explore the possible origin, we have used phase field method to simulate the structure of strip-shape R-BFO embedded in T-BFO matrix with unstable reversed domains (**Figure 4**b), which is based on the experimental domain structure measured by PFM (Figure 4a). The calculated elastic energy density is plotted in Figure 4c, while the elastic energy along the diagonal, the direction of arrow in Figure 4c, is given in Figure 4d. The simulation results indicate that the elastic energy shows periodic spatial distribution in the mixed-phase region. In Figure 4c and 4d, the elastic energy density is higher in the strained T-BFO matrix than that in the mixed-phase region, which explains the experimental results of longer relaxation time for reversed domains in the mixed-phase region. Note that the distribution of elastic energy does not change after the reversed domains are written or relaxed, because both T and –T variants (also R and -R variants) possess the same transformation strain. This is consistent with the unchanged topography observed in Figure 1 with regardless of the relaxation of domains. In the reversed domain, both out-of-plane and in-plane PFM components had phase contrasts opposite to the as-grown state (see supporting information, Figure S1), which means that the domain performed an 180° ferroelectric polarization switching from the as-grown domain without changing the strain distribution. However, strain components were slightly twisted at the domain walls (Figure S1), so we can simplify the problem as moving domain walls in the elastic potential landscapes provided by the as-grown phase structures. Figure 4c and 4d show that the distribution of elastic energy has wells at T/R phase boundaries. This result suggests that the mixed-phase region supplies the basic potential well structure for reversed domain pinning, which agrees with the experimental observations of T/R phase boundaries acting as domain-wall pinning centers.

Based on the results from phase field simulation, we have further used the concept to improve the domain retention. We have found out that when a reversed domain is smaller than 100 nm, the domain relaxation rate depends on its relative position to the as-grown mixed-phase stripes. In **Figure 5**, three kinds of reversed domains were all switched in the mixed phase region by external voltage pulses with a tip bias of –12 V and

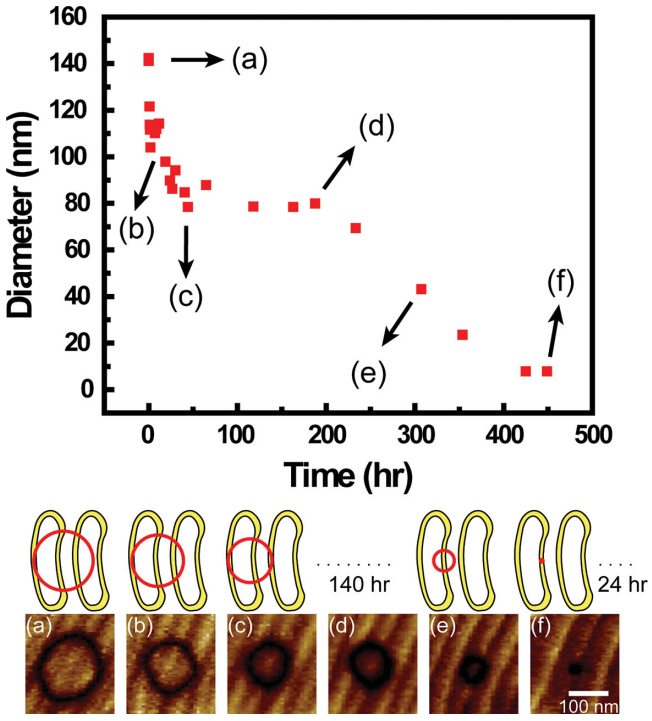

Figure 3. a) to f) Different stages for a reversed domain with initial diameter about 140 nm relaxing toward the as-grown state in the mixed-phase region. (Top) Domain diameters versus the relaxation time. (Bottom) OP PFM amplitude images of different relaxation stages corresponding to stages (a) to (f). The middle diagram illustrates the evolution of domain structures of the reversed domain (circle) in the mixed-phase strip boundaries (curved loops).

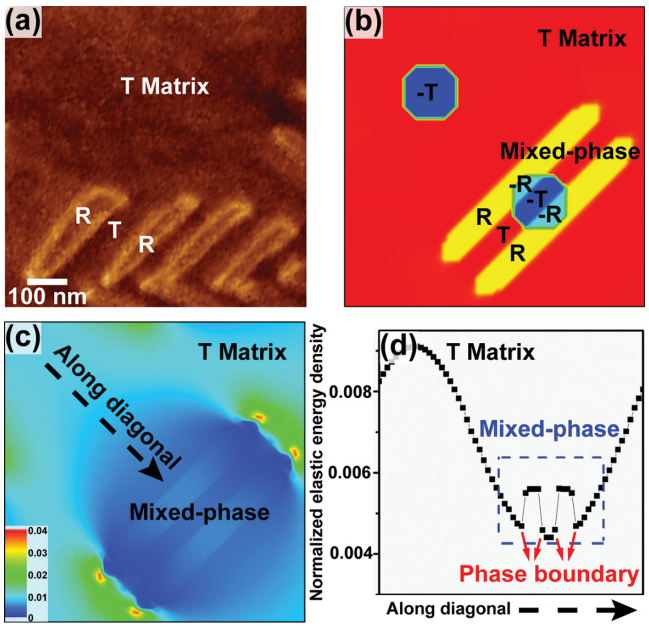

Figure 4. a) OP PFM amplitude images of domains in as-grown film. b) Phase field simulation structure of R-BFO embedded in T-BFO matrix with written reversed domains, and c) the distribution of normalized elastic energy density corresponding to (b); d) the normalized elastic energy density along one diagonal in (c).

pulse duration of 100 ms. With different locations and initial sizes, these domains have various retention behaviors. The relaxation times of different processes were determined by fitting the relaxation curves using exponential decay functions. For the first case in Figure 5a, the OP-PFM amplitude images show that the reversed domain was initially created on a mixed-phase stripe, with its domain wall staying symmetrically across a closed loop of the phase boundary. Both left and right sides of the domain wall relaxed to the nearest T/R-phase boundaries quickly (within 48 hr), and then the reversed domain maintained at this stable state for a long time. After our testing period, the domain in Figure 5a was still larger than half of its initial size, so we can conclude its relaxation time is much longer than 327 hr. This case shows the longest retention. For the second case in Figure 5b, the reversed domain was initially located half inside and half outside a mixed-phase boundary loop. Both left and right sides of its initial domain wall were located near as-grown boundaries, and there was another phase boundary at the center of the domain. This reversed domain was also relatively stable, but finally it relaxed slowly with the domain wall moving toward the center phase boundary. Compared to the first-case domain, the relaxation time of this domain is shorter (~327 hr). It should be noted that the relaxation curve of the second-case domain is similar to the late relaxation stage of the larger reversed domain in Figure 3. For the third case in Figure 5c, the domain configuration is similar to that in Figure 5b, but the initial reversed domain diameter is smaller (~65 nm) than that of the second-case domain (~80 nm). At the beginning, neither side of this reversed domain wall was located on T/R-phase boundaries. The domain wall then quickly moved toward the phase boundary near the center of the reversed domain, with the relaxation time of only ~50 hr. Comparing domains in Figure 5b and 5c, we can see that the initial domain size larger than the width of the mixed-phase stripe is a required condition for the domain to reach a stable state.

Above experimental results indicate that the T/R phase boundaries are local pinning sites for the domain wall motion, and the phase-field simulation shows that this is because the elastic energy increases when the domain wall moves away from the T/R phase boundary. To simplify the concept, the model potential diagrams for the domain wall motion of the three relaxation cases are correspondingly shown in Figure 5. The dot lines, U_S, include local elastic potential minima of the domain wall at T/R phase boundaries while the dash lines, U_D, illustrate the potential related to the field driving the domain wall relaxing toward the domain center. The relaxation-driving field is mainly contributed from the unscreened depolarization fields due to the asymmetrical out-of-plane boundaries, and the width of U_D well gives the domain diameter. Combining the effects from U_D and U_S, the resultant potential energy diagrams in Figure 5 explain the domain relaxation processes of three different cases. For the case of Figure 5a, the resultant potential is spatially symmetric, with two local minima locating on phase boundaries across the center. When domain walls moved from the initial positions to these pining sites, the domain reached a low-energy stable state. For the case of Figure 5b, the energy minimum of the domain wall is at the center. Although the domain wall was pinned by phase boundaries for a while,

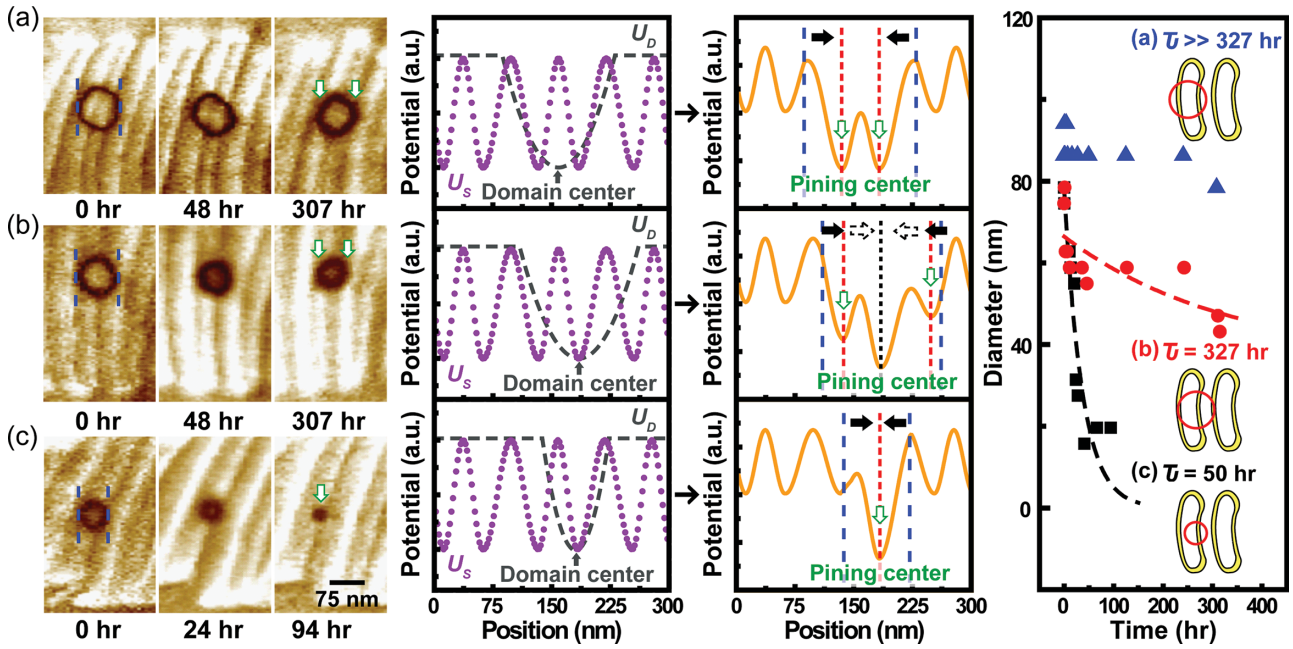

Figure 5. Domain relaxation behaviors and model diagrams of three reversed domains with different initial locations. a) The domain located symmetrically across a mixed-phase strip had longest retention. b) The domain with the center near one mixed-phase boundary and with the domain wall on two mixed-phase boundaries gradually shrank toward the center boundary. c) The domain with the center near one mixed-phase boundary and with the domain wall unpinned quickly shrank toward the center boundary. (Left) Out-of-plane PFM amplitude images versus relaxing time. (Center) Model diagram of potential energy versus the domain wall positions. The solid arrows in the resultant diagram indicate the domain wall motion from initial positions to pinning centers, which are pointed by hollow arrows. (Right) Domain diameters versus the relaxing time for (a), (b), and (c) domains.

eventually the domain relaxed toward the center. For the case of Figure 5c, the initial domain wall was unpinned, so the domain relaxed to the as-grown state quickly. Writing the nano-domain in a symmetric configuration as Figure 5a demonstrates an easy way to create stable state of reversed domain by using the in-plane periodic potentials. Figure 5 also shows that the minimum diameter of a stable domain depends on the periodicity of the stripe phases, which is about 80 nm of our studied sample. Based on this stable domain size, the estimation of maximum storage density is of the order about 10 Gbit/cm^2. The periodicity of the stripes can be further reduced by changing the substrate strain or the film thickness, and the storage density of one order higher is obtainable. For non-volatile device application, increasing the strain gradient or reducing the depolarization field are both directions to enhance the domain pinning effects. For example, applying a suitable voltage to inject screen charges but not to change the phase structure is a possible way to improve this system.

In summary, we observed a giant enhancement of retention in the mixed-phase region of a strained BFO film. The T/R mixed-phase boundaries act as pinning centers of domain walls in the relaxation process. By taking the advantages of periodic potential distribution due to the mixed-phase strips, we demonstrated a simple method to create long-retention reversed domain. When a reversed domain is symmetrically placed across a mixed-phase stripe, the symmetric potential minima can pin the domain in a stable state. Compared to the reversed domains written by SPM tips in other ferroelectrics, the symmetric potential design based on the BFO periodic strain opens a new avenue to the application of nano-sized, nonvolatile electronic devices.

Experimental Section

The mixed-phase $BiFeO_3$ (BFO) film was epitaxially grown on a (001) $LaAlO_3$ (LAO) substrates by pulsed laser deposition assisted with high-pressure reflection high energy electron diffraction (RHEED). The BFO film is 150 nm in thickness, and a thin conducting $LaNiO_3$ layer of 15 nm was inserted as the bottom electrode. The topography and the domain structure of the film were examined by a commercial scanning probe microscope (SPM) (Multimode, Bruker). Nano-domains were created by applying voltage pulses on the film with SPM tips. The evolution of domain structures was tracked by piezoresponse force microscopy (PFM) using a Pt-Ir coated tip with elastic constant about 7 N/m and an ac modulation voltage of 1.0 V at 6.39 kHz. The lateral resolution of PFM imaging is about 6 nm. The elastic energy distribution of the sample was calculated using the phase field simulation, which was carried out using characteristic functions of variants as variables, as detailed in the previous work.[42]

Supporting Information

Supporting Information is available from the Wiley Online Library or from the author.

Acknowledgements

The work at National Cheng Kung University is supported by Ministry of Science and Technology, R.O.C. (NSC 102–2112-M-006 -008 -MY3) and the Headquarters of University Advancement at National Cheng Kung University, which is sponsored by the Ministry of Education, Taiwan, R.O.C. The work at National Chiao Tung University is supported by Ministry of Science and Technology, R.O.C.

(NSC-101–2119-M-009–003-MY2), Ministry of Education (MOE-ATU 101W961), and Center for interdisciplinary science of National Chiao Tung University. YYL acknowledges the support of NSFC (11102175), and JYL acknowledges the support of NSF (CMMI-1100339).
Note: The names of the authors Yunya Liu and Jiangyu Li in the author line were corrected on September 24, 2014.

Received: June 2, 2014
Revised: July 2, 2014
Published online: August 11, 2014

[1] E. Y. Tsymbal, H. Kohlstedt, *Science* **2006**, *313*, 181.
[2] A. Chanthbouala, A. Crassous, V. Garcia, K. Bouzehouane, S. Fusil, X. Moya, J. Allibe, B. Dlubak, J. Grollier, S. Xavier, C. Deranlot, A. Moshar, R. Proksch, Ne. D. Mathur, M. Bibes, A. Barthélémy, *Nat. Nanotechnol.* **2012**, *7*, 101.
[3] P. Maksymovych, S. Jesse, P. Yu, R. Ramesh, A. P. Baddorf, S. V. Kalinin, *Science* **2009**, *324*, 1421.
[4] V. Garcia, S. Fusil, K. Bouzehouane, S. Enouz-Vedrenne, N. D. Mathur, A. Barthélémy, M. Bibes, *Nature* **2009**, *460*, 81.
[5] A. Gruverman, D. Wu, H. Lu, Y. Wang, H. W. Jang, C. M. Folkman, M. Ye. Zhuravlev, D. Felker, M. Rzchowski, C. B. Eom, E. Y. Tsymbal, *Nano Lett.* **2009**, *9*, 3539.
[6] V. Garcia, M. Bibes, L. Bocher, S. Valencia, F. Kronast, A. Crassous, X. Moya, S. Enouz-Vedrenne, A. Gloter, D. Imhoff, C. Deranlot, N. D. Mathur, S. Fusil, K. Bouzehouane, A. Barthélémy, *Science* **2010**, *327*, 1106.
[7] S. Valencia, A. Crassous, L. Bocher, V. Garcia, X. Moya, R. O. Cherifi, C. Deranlot, K. Bouzehouane, S. Fusil, A. Zobelli, A. Gloter, N. D. Mathur, A. Gaupp, R. Abrudan, F. Radu, A. Barthélémy, M. Bibes, *Nat. Mater.* **2011**, *10*, 753.
[8] P. Maksymovych, A. N. Morozovska, P. Yu, E. A. Eliseev, Y. H. Chu, R. Ramesh, A. P. Baddorf, S. V. Kalinin, *Nano Lett.* **2012**, *12*, 209.
[9] Y. C. Chen, C. H. Ko, Y. C. Huang, J. C. Yang, Y. H. Chu, *J. Appl. Phys.* **2012**, *112*, 052017.
[10] D. D. Fong, A. M. Kolpak, J. A. Eastman, S. K. Streiffer, P. H. Fuoss, G. B. Stephenson, C. Thompson, D. M. Kim, K. J. Choi, C. B. Eom, I. Grinberg, A. M. Rappe, *Phys. Rev. Lett.* **2006**, *96*, 127601.
[11] S. Zhong, S. P. Alpay, J. V. Mantese, *Appl. Phys. Lett.* **2005**, *87*, 102902.
[12] N. Sai, B. Meyer, D. Vanderbilt, *Phys. Rev. Lett.* **2000**, *84*, 5636.
[13] S. J. Callori, J. Gabel, D. Su, J. Sinsheimer, M. V. Fernandez-Serra, M. Dawber, *Phys. Rev. Lett.* **2012**, *109*, 067601.
[14] T. H. Kim, S. H. Baek, S. M. Yang, S. Y. Jang, D. Ortiz, T. K. Song, J.-S. Chung, C. B. Eom, T. W. Noh, J.-G. Yoon, *Appl. Phys. Lett.* **2009**, *95*, 262902.
[15] R. J. Zeches, M. D. Rossell, J. X. Zhang, A. J. Hatt, Q. He, C. H. Yang, A. Kumar, C. H. Wang, A. Melville, C. Adamo, G. Sheng, Y. H. Chu, J. F. Ihlefeld, R. Erni, C. Ederer, V. Gopalan, L. Q. Chen, D. G. Schlom, N. A. Spaldin, L. W. Martin, R. Ramesh, *Science* **2009**, *326*, 977.
[16] H. J. Liu, C. W. Liang, W. I. Liang, H. J. Chen, J. C. Yang, C. Y. Peng, G.-F. Wang, F. N. Chu, Y. C. Chen, H. Y. Lee, L. Chang, S. J. Lin, Y. H. Chu, *Phys. Rev. B* **2012**, *85*, 014104.
[17] A. R. Damodaran, S. Lee, J. Karthik, S. MacLaren, L. W. Martin, *Phys. Rev. B* **2012**, *85*, 024113.
[18] I. C. Infante, J. Juraszek, S. Fusil, B. Dupé, P. Gemeiner, O. Diéguez, F. Pailloux, S. Jouen, E. Jacquet, G. Geneste, J. Pacaud, J. Íñiguez, L. Bellaiche, A. Barthélémy, B. Dkhil, M. Bibes, *Phys. Rev. Lett.* **2011**, *107*, 237601.
[19] A. R. Damodaran, C. W. Liang, Q. He, C. Y. Peng, L. Chang, Y. H. Chu, L. W. Martin, *Adv. Mater.* **2011**, *23*, 3170.
[20] J. X. Zhang, Q. He, M. Trassin, W. Luo, D. Yi, M. D. Rossell, P. Yu, L. You, C. H. Wang, C. Y. Kuo, J. T. Heron, Z. Hu, R. J. Zeches, H. J. Lin, A. Tanaka, C. T. Chen, L. H. Tjeng, Y. H. Chu, R. Ramesh, *Phys. Rev. Lett.* **2011**, *107*, 147602.
[21] C. Beekman, W. Siemons, T. Z. Ward, M. Chi, J. Howe, M. D. Biegalski, N. Balke, P. Maksymovych, A. K. Farrar, J. B. Romero, P. Gao, X. Q. Pan, D. A. Tenne, H. M. Christen, *Adv. Mater.* **2013**, *25*, 5561.
[22] Q. He, Y. H. Chu, J. T. Heron, S. Y. Yang, W. I. Liang, C. Y. Kuo, H. J. Lin, P. Yu, C. W. Liang, R. J. Zeches, W. C. Kuo, J. Y. Juang, C. T. Chen, E. Arenholz, A. Scholl, R. Ramesh, *Nat. Commun.* **2011**, *2*, 225.
[23] Y. C. Chen, Q. He, F. N. Chu, Y. C. Huang, J. W. Chen, W. I. Liang, R. K. Vasudevan, V. Nagarajan, E. Arenholz, S. V. Kalinin, Y. H. Chu, *Adv. Mater.* **2012**, *25*, 5561.
[24] J. Zhou, M. Trassin, Q. He, N. Tamura, M. Kunz, C. Cheng, J. Zhang, W. I. Liang, J. Seidel, C. L. Hsin, J. Wu, *J. Appl. Phys.* **2012**, *112*, 064102.
[25] P. Paruch, T. Giamarchi, J.-M. Triscone, *Phys. Rev. Lett.* **2005**, *94*, 197601.
[26] J. Guyonnet, I. Gaponenko, S. Gariglio, Patrycja Paruch, *Adv. Mater.* **2011**, *23*, 5377.
[27] S. F. Liu, Y. J. Wu, J. Li, X. M. Chen, *Appl. Phys. Lett.* **2014**, *104*, 5.
[28] A. N. Morozovska, E. A. Eliseev, G. S. Svechnikov, S. V. Kalinin, *J. Appl. Phys.* **2013**, *113*, 9.
[29] H. H. Wu, J. Wang, S. G. Cao, L. Q. Chen, T. Y. Zhang, *J. Appl. Phys.* **2013**, *114*, 9.
[30] P. Gao, C. T. Nelson, J. R. Jokisaari, S. H. Baek, C. W. Bark, Y. Zhang, E. G. Wang, D. G. Schlom, C. B. Eom, X. Q. Pan, *Nat. Commun.* **2011**, *2*, 6.
[31] W. Ren, Y. Yang, O. Diéguez, J. Íñiguez, N. Choudhury, L. Bellaiche, *Phys. Rev. Lett.* **2013**, *110*, 187601.
[32] T. K. Song, J. G. Yoon, S. I. Kwun, *Ferroelectrics* **2006**, *335*, 61.
[33] D. S. Fu, K. Suzuki, K. Kato, H. Suzuki, *Appl. Phys. Lett.* **2003**, *82*, 2130.
[34] Y. Kan, X. Lu, H. Bo, F. Huang, X. Wu, J. Zhu, *Appl. Phys. Lett.* **2007**, *91*, 132902.
[35] J. W. Hong, W. Jo, D. C. Kim, S. M. Cho, H. J. Nam, H. M. Lee, J. U. Bu, *Appl. Phys. Lett.* **1999**, *75*, 3186.
[36] C. S. Ganpule, V. Nagarajan, S. B. Ogale, A. L. Roytburd, E. D. Williams, R. Ramesh, *Appl. Phys. Lett.* **2000**, *77*, 3275.
[37] A. Gruverman, H. Tokumoto, A. S. Prakash, S. Aggarwal, B. Yang, M. Wuttig, R. Ramesh, O. Auciello, T. Venkatesan, *Appl. Phys. Lett.* **1997**, *71*, 3492.
[38] H. R. Zeng, K. Shimamura, E. G. Villora, S. Takekawa, K. Kitamura, *J. Appl. Phys.* **2007**, *101*, 074109.
[39] A. Gruverman, M. Tanaka, *J. Appl. Phys.* **2001**, *89*, 1836.
[40] C. S. Ganpule, A. L. Roytburd, V. Nagarajan, B. K. Hill, S. B. Ogale, E. D. Williams, R. Ramesh, *Phys. Rev. B* **2001**, *65*, 014101.
[41] V. V. Shvartsman, A. L. Kholkin, M. Tyunina, J. Levoska, *Appl. Phys. Lett.* **2005**, *86*, 222907.
[42] Y. Y. Liu, R. K. Vasudevan, K. Pan, S. H. Xie, W.-I. Liang, A. Kumar, S. Jesse, Y.-C. Chen, Y.-H. Chu, V. Nagarajan, S. V. Kalinin, J. Y. Li, *Nanoscale* **2012**, *4*, 3175.